Band structure of $CdGeAs_2$ near the fundamental gap

Sukit Limpijumnong*
School of Physics, Institute of Science, Suranaree University of Technology, Nakhon Ratchasima 30000, Thailand

Walter R. L. Lambrecht
Department of Physics, Case Western Reserve University, Cleveland, Ohio 44106-7079
(Received 25 October 2001; published 4 April 2002)

First-principles band structure calculations were carried out for the chalcopyrite semiconductor $CdGeAs_2$ using the linear muffin-tin orbital method, including spin-orbit coupling. The emphasis of the analysis is on the band gaps and energy band splittings near the fundamental gap. The gap underestimate due to the local-density approximation is corrected using information on quasiparticle calculations for the parent compound GaAs. The experimental information on optical transitions near the gap is reviewed critically in the light of our calculations. The polarization dependence and the pseudodirect nature of some of the transitions is discussed. The effective masses of the conduction band and valence bands are derived from the calculated band structure. A generalization of the Luttinger Hamiltonian for chalcopyrite is presented and its parameters determined.

DOI: 10.1103/PhysRevB.65.165204 PACS number(s): 71.20.Nr, 71.35.Cc

I. INTRODUCTION

Among the ternary semiconductor compounds with chalcopyrite (CKP) structure, $CdGeAs_2$ is one of the most promising ones for nonlinear optical frequency conversion because of its record value of the second harmonic generation coefficient $\chi^{(2)} \approx 350-500$ pm/V.[1–3] Recently, there has been renewed interest in improving the crystal growth of this material and in determining its fundamental properties, in particular the band structure, defect, and optical properties.[4–6] On the experimental side, several studies of the optical transitions were reported several decades ago, using various techniques.[7–13] On the theoretical side, there have been only a few attempts to calculate the band structure and a detailed knowledge is still lacking. The earliest band structure study by Zlatkin *et al.*[14] did not include spin-orbit interactions and was limited to a few **k** points.[14] Later work by Polygalov *et al.*[15] did include the spin-orbit interaction but still was limited to only three **k** points.[15] Madelon *et al.*[16] reported the first more complete empirical pseudopotential calculations along symmetry directions of the Brillouin zone (BZ) and also included spin-orbit interactions. To our knowledge the first calculation in the framework of density functional theory was by Zapol *et al.*[17] Their calculations, however, do not include spin-orbit coupling and focus primarily on structural properties. They do not provide information about the optical transitions. Rashkeev *et al.*[3] also performed local density approximation band structure calculations (using the linear muffin-tin orbital method) and reported calculations of the linear and second order optical response functions but did not describe the details of the band structure near the fundamental gap.

Here, we use a first-principles approach in which the only experimental input consists of the crystal stucture parameters (a, c/a, and u), except that some corrections are applied to overcome the well-known band gap underestimate of the local density approximation (LDA). We have earlier reported a similar study of another CKP semiconductor $ZnGeP_2$.[18] Our approach is, in fact, similar to the one followed in that paper. Namely, we exploit the similarity of the chalcopyrite semiconductors to their III-V parent compound, for example GaP for $ZnGeP_2$. Since adequate experimental information as well as quasiparticle calculations in the GW approximation are available[19] for the conduction bands at various **k** points and the relation of these states to those in the chalcopyrite by BZ folding are well understood, it is relatively straightforward to estimate the corrections to the important states near the fundamental gap in the chalcopyrite material. The details about the relation (band folding) between the zinc blende (ZB) and chalcopyrite structures can be found in our earlier paper on $ZnGeP_2$ and GaP.[18] In the case of $ZnGeP_2$, these corrections do not significantly affect the effective masses or valence band maximum effective Hamiltonian parameters because the experimental minimum gap is ~ 2.2 eV and the LDA gives a value of 1.1 eV. Thus those parameters could be safely obtained from the LDA band structure and only when it comes to judging the direct *versus* indirect nature of the band gap and optical properties, the corrections had to be invoked. In the case of $CdGeAs_2$, the problem is more severe because in the LDA, we obtain a negative gap. Several experiments reported the band gap to be ~ 0.6 eV.[7–11,16] We note that the LDA calculations of Zapol *et al.*[17] obtained a small but positive gap. The reason is most likely the use of an incomplete basis set. The result of our negative gap is that the topology of the bands, i.e., the way they are connected, near Γ is strongly distorted and meaningful effective mass information cannot be obtained from the LDA bands directly. In order to extract any useful information at the band edges, we need to adjust the Hamiltonian matrix and recalculate the band structure including corrections beyond LDA. Details of how we accomplish this are discussed in Sec. II

The rest of the paper is organized as follows. In the results section, we first discuss the band structures and splittings at Γ in Sec. III A. Then we relate this to the optical transitions in Sec. III B. Next, we discuss the effective masses in the conduction band in Sec. III C and the effective mass Hamiltonian for the valence band maximum (VBM) in III D.

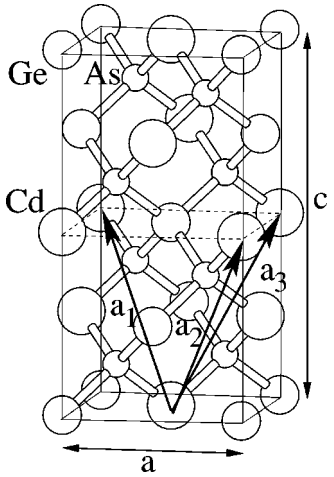

FIG. 1. The chalcopyrite crystal structure.

II. COMPUTATIONAL METHOD

Since we are here primarily interested in the band structure, we choose to perform all calculations at the experimental lattice parameters $a=5.945$ Å, $c/a=1.887$, and $u=0.285$ (Ref. 20) rather than optimizing the structural parameters using the first-principles approach. We thus avoid the typical underestimate of the lattice constant due to the overbinding of the LDA. The CKP crystal structure is shown in Fig. 1. It is a superlattice of the ZB structure with a specific ordered arrangement of the Cd and Ge cations accompanied by small structural distortions. It can be described in a body centered tetragonal primitive unit cell. The corresponding lattice vectors $\mathbf{a}_1=(-a/2,a/2,c/2)$, $\mathbf{a}_2=(a/2,-a/2,c/2)$, and $\mathbf{a}_3=(a/2,a/2,c/2)$ are indicated in Fig. 1. The structural parameters are the a lattice constant, the c/a ratio, and the internal structural parameter u, which determines the position of the anion in its nearest neighbor tetrahedron. For example, the atom in the lower left corner has coordinates $(a/4,ua,c/8)$. In the ideal structure $c/a=2$ and $u=1/4$.

We use the density functional theory (DFT) in the local density approximation (LDA) (Ref. 21) as parametrized by Hedin and Lundqvist.[22] The linear muffin-tin orbital (LMTO) method was used both in the full-potential (FP) implementation of Methfessel[23] and in the atomic sphere approximation (ASA). The FP method uses nearly touching muffin-tin radii with empty spheres inserted in the usual interstitial sites for a tetrahedrally coordinated material. The Cd $4d$ orbitals are treated as valence bands, while the deeper Ge $3d$ orbitals are treated as core states. The angular momentum cut-off used for the interstitial region Hankel function basis set is $l_{\max}=6$. Brillouin zone integration was carried out with a regularly spaced mesh of $8\times8\times8$ points in the reciprocal unit cell shifted from the origin as in the Monkhorst-Pack method[24] and reduced by symmetry to a set of irreducible **k** points. For the calculations of the spin-orbit splitting and the gap corrections, to be discussed below, we used the atomic sphere approximation to the LMTO method[25] after checking that the ASA results without spin-orbit coupling were in good agreement with the full-potential results for the bands of interest. Since spin-orbit coupling arises primarily from the inner part of the atomic spheres, where the potential is very close to being spherically symmetric, this should be an adequate approximation.

Strictly speaking, the eigenvalues of the Kohn-Sham equation are not the quasiparticle eigenenergies but only intermediate results in the total energy calculation. However, the quasiparticle equation differs from the Kohn-Sham equation only in that the exchange correlation potential should be replaced by a nonlocal and energy dependent exchange correlation self-energy operator. This leads to a well known underestimation of the band gaps. In most cases in wide-bandgap semiconductors, LDA gaps are still resonably large and useful information near the band edges can immediately be extracted from pure first-principle results. Unfortunately, for the case at hand the experimental gap is small (~0.6 eV) and the LDA gap is negative. In order to investigate the band edges, it is imperative to modify the Hamiltonian so as to shift up the conduction band (CB) that is crossing with the valence band (VB).

In the LMTO-ASA method the Hamiltonian has essentially a two-center tight-binding form[25]

$$H_{RL,R'L'}(\mathbf{k})=C_{Rl}\delta_{RL,R'L'}+\sqrt{\Delta_{Rl}}S_{RL,R'L'}(\mathbf{k})\sqrt{\Delta_{R'l'}}, \tag{1}$$

in which $S_{RL,R'L'}(\mathbf{k})$ is the structure constant matrix, RL label the atomic sites R and angular momenta $L=lm$ of the basis set, and C_{Rl} and Δ_{Rl} are potential parameters that determine, respectively, the ''center of the Rl band'' and the ''width of the bands.'' To be precise, this Hamiltonian in the so-called ''nearly orthogonal representation'' is correct to second order in $(E-E_\nu)$ with E_ν the linearization energy of the LMTO method. In reality, we include further three-center correction terms and third-order corrections but these are irrelevant for the present purpose of explaining our gap correction method. The point is that by simply shifting the C_{Rl} we can modify the position of the center of the Rl band. It turns out that the conduction band minimum at Γ in tetrahedrally bonded semiconductors has primarily cation s character, while the valence band maximum has primarily anion p character. In the ASA, we introduce empty spheres at the tetrahedral interstices to fill space with spheres which are not too much overlapping. The wave functions then also contain expansions in muffin tin orbitals centered at these empty sites. The empty sphere s basis states also have a large contribution to the first few conduction band states, and in particular strongly influence the position of the state at X (of zinc blende BZ). Since in chalcopyrite the states at X become folded at Γ, the first two conduction bands at X determine the position of the second and third conduction band at Γ for a direct gap situation. Experience has shown that shifting of the empty sphere and cation s states by a few 0.1 Ry shifts the conduction bands up by the order of an eV without significantly modifying the valence bands. Thus we can semiempirically determine the necessary shifts to obtain a target band gap at X and Γ. In the process, the gaps at other **k** points also improve systematically because they have a wave function basis set composition intermediate between those states.

TABLE I. Selected conduction band eigenvalues measured from the VBM in $CdGeAs_2$ and GaAs in eV.

		GaAs			$CdGeAs_2$		
ZB	CKP	LDA [a]	GW [a]	GW-LDA	LDA	LDA+ [b]	LDA++ [c]
Γ_1	Γ_1	0.67	1.58	0.91	−0.47	0.44	0.60
$X_1(z)$	Γ_3	1.49	2.19	0.70	1.09	1.79	1.79
$X_3(z)$	Γ_2	1.66	2.41	0.75	1.50	2.25	2.25

[a]Reference 26.

[b]LDA with corrections extracted from GaAs (column 6 + column 5).

[c]LDA with corrections extracted from GaAs and additional correction on Γ_1 based on the LDA location of Cd-4*d*; see text for detail.

The question then remains what corrections we should expect. For that purpose, we again consider the parent III-V compounds. In the case of $CdGeAs_2$ it is not clear *a priori* whether we should consider InAs or GaAs or some $InGaAs_2$ alloy as the parent compound. However, it turns out that this is irrelevant because very similar upward shifts of the In *s* and Ga *s* and corresponding empty spheres *s* can be used to correct the gaps in both InAs and GaAs and the gap corrections themselves are also similar. Because more detailed results of quasiparticle calculations are available for GaAs than for InAs we chose to base our correction on those of GaAs. The band gap corrections in GaAs at the Γ and *X* points are taken from the quasiparticle calculations of Refs. 26,27, which agree closely between each other. They show that the Γ_{1c} state shifts up by 0.91 eV relative to the Γ_{15v} (the VBM), while the X_{1c} and X_{3c} states shift by, respectively, 0.70 and 0.75 eV. We then assume that the Γ_{1c} is also shifted by 0.91 eV and the Γ_{2c} and Γ_{3c} are shifted by 0.75 and 0.70 eV in $CdGeAs_2$ because they are their chalcopyrite folded counterparts. We then determine the shifts of the C_{Rl} of the cation *s* and empty sphere *s* necessary to obtain the target shifts of the conduction bands. In fact, we find that the first three CB's have both Cd *s* and Ge *s* components and thus we apply the same shift to all cation states. In addition, the first two higher CB's as expected because they are folded *X* states, have large empty sphere (ES) type I *s* component; the second higher CB also has in addition a large ES type II component. Type I and II refer to the nearest neighbors of the empty sphere which are cations for type I and anions for type II. We can therefore adjust each CB by changing the LMTO potential parameters associated with the states that are dominant for the particular band. Since we have three adjustable parameters, i.e., the shifts of the cation *s* and the two types of empty spheres, and there are three shifts to fit, it is straightforward to find a unique solution for the three shifts since the gaps vary linearly with the potential shifts.

The results are (see Table I) still not entirely satisfactory for the minimum conduction band. It predicts a band gap of $CdGeAs_2$ of only 0.44 eV compared to the experimental gap of ~ 0.6 eV. We believe the remaining discrepancy is due to the effects of the Cd 4*d* band which lies at about -9 eV below the VBM. One expects that the quasiparticle corrections will shift this state down by about 1 eV. Because it hybridizes with the VBM which forms antibonding states with it, a downward shift of the Cd 4*d* will result in a downward shift of the VBM. However, inspection of the eigenvectors reveals that the Γ_{2c} and Γ_{3c} states have similar *d* contributions to those of the valence band maximum. Therefore we expect the Γ_{2c} and Γ_{3c} states to shift along with the VBM relative to the Γ_{1c} state. This means that only the minimum gap is expected to further increase from what we expect on the basis of GaAs. Our approach has been to adjust the minimum gap $\Gamma_{1c}-\Gamma_{4v}$ to a value of 0.6 eV as suggested by experiment.

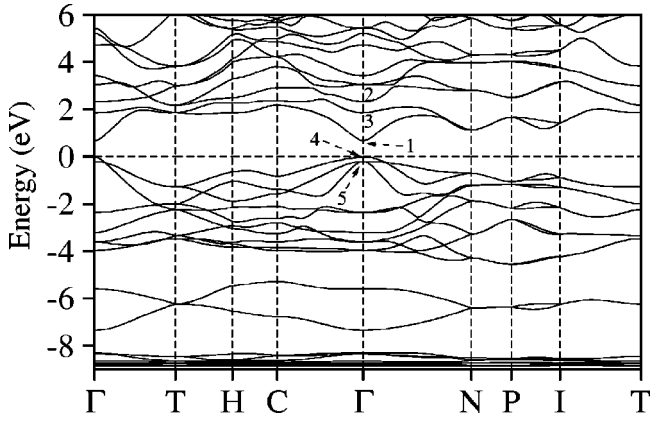

FIG. 2. Band structure of $CdGeAs_2$ in the local density approximation without spin-orbit interaction at experimental lattice parameters. The first three CB have been shifted up according to the corrections obtained from available GW results on GaAs as explained in text.

We emphasize that these corrections leave the valence band splittings essentially unchanged so we can consider these splittings as first-principles results. Also, the shifts at the gaps at other **k** points were not adjusted and can be considered ''first-principles'' predictions once we have adjusted our Hamiltonian.

III. RESULTS

A. Band structures

The band structure of $CdGeAs_2$ without spin-orbit interaction is shown in Fig. 2. The symmetry **k** points are labeled following Ref. 18. The corresponding BZ is shown in Fig. 3 along with that of ZB for comparison. The band structure including spin-orbit coupling is shown along the Γ-*T* and Γ-*N* lines in Fig. 4.

$CdGeAs_2$ has a direct band gap at Γ. The next higher local minimum is at *N*, 0.45 eV higher. In Fig. 2, the most relevant states are labeled according to their irreducible symmetry representations following the character table given by Sandrock and Treusch,[28] which coincide with the well-known tables of Koster *et al.*[29]

The lower three CB states counting from the CBM are Γ_1, Γ_3, and Γ_2. Our ordering of the two higher CB is reversed from that of Madelon *et al.*[16] and Zlatkin *et al.*[14] but in agreement with Polygalov *et al.*[15] The energy splitting between Γ_2 and Γ_3 is 0.46 eV, larger than -0.20 eV (the minus sign indicates that the Γ_{3c} state lies above the Γ_{2c} state) predicted by Madelon *et al.*[16]

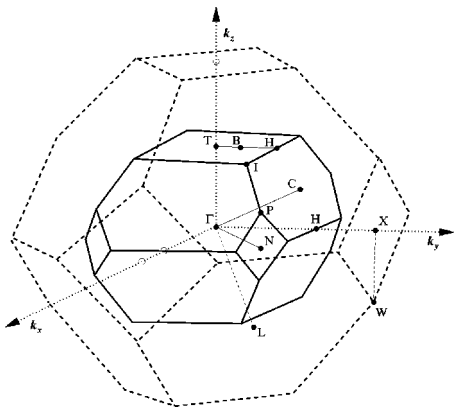

FIG. 3. First Brillouin zone (BZ) of chalcopyrite structure (solid lines) and its relation to that of the zinc blende (ZB) structure (dashed lines). The points *X*, *L*, and *W* lie on the ZB BZ.

When the spin-orbit interaction is not included in the calculation, we find the singlet (Γ_4) is lying above the doublet (Γ_5) with the splitting (crystal-field splitting Δ_c) of -205 meV (the minus sign indicates that the singlet lies above the doublet). When the spin-orbit interaction is included in our calculations (the band structures is shown in Fig. 4), we use double group notation according to Refs. 28,30: $\Gamma_5 \rightarrow (\Gamma_6, \Gamma_7)$, $\Gamma_1 \rightarrow \Gamma_6$, $\Gamma_2 \rightarrow \Gamma_6$, $\Gamma_3 \rightarrow \Gamma_7$, and $\Gamma_4 \rightarrow \Gamma_7$. Below, we will use a notation $\Gamma_7(4)$ to indicate the Γ_7 state derived mainly from the Γ_4.

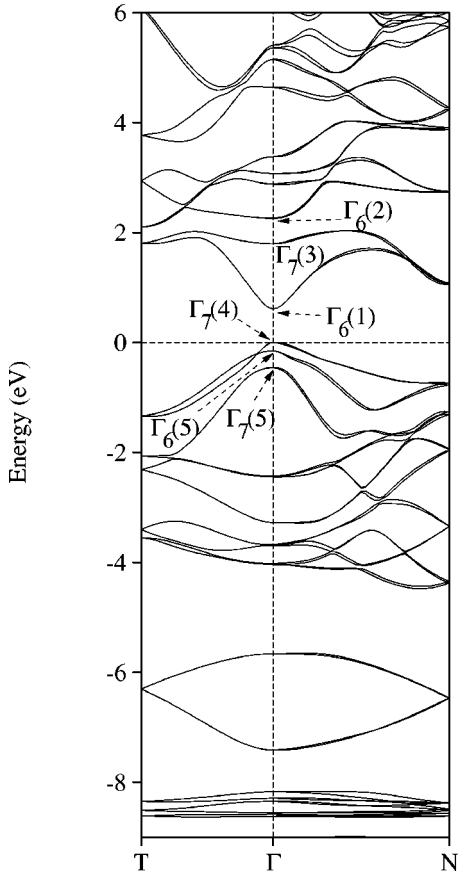

FIG. 4. Band structure of $CdGeAs_2$ in the local density approximation with spin-orbit interaction at experimental lattice parameters. The first three CB have been shifted up according to the corrections obtained from available GW results on GaAs as explained in text.

The splittings at Γ can be described by the Hamiltonian

$$H = \Delta_c L_z^2 + \Delta_s^{\parallel} L_z \sigma_z + \Delta_s^{\perp} (L_x \sigma_x + L_y \sigma_y), \tag{2}$$

which leads to the eigenvalues

$$\Gamma_6(5) = \Delta_c + \Delta_s^{\parallel},$$

$$\Gamma_7\left(\frac{5}{4}\right) = \frac{\Delta_c - \Delta_s^{\parallel}}{2} \pm \sqrt{\left(\frac{\Delta_c - \Delta_s^{\parallel}}{2}\right)^2 + 2\Delta_s^{\perp 2}}. \tag{3}$$

The crystal field splitting Δ_c is obtained from the calculation without spin-orbit coupling. The first-principles calculation including spin-orbit coupling provides us with two energy differences in Eq. (3) from which we can extract both $\Delta_s^{\parallel}$ and $\Delta_s^{\perp}$. This gives

$$\Delta_c = -205 \text{ meV},$$

$$\Delta_s^{\parallel} = 114 \text{ meV}, \quad \Delta_s^{\perp} = 119 \text{ meV}.$$

In fact, to a very good approximation, the quasicubic model in which $\Delta_s^{\parallel} = \Delta_s^{\perp} = \Delta_s/3$ holds. If we make this assumption and fit the two energy splittings directly we obtain $\Delta_s = 356$ meV and $\Delta_c = -196$ meV. The magnitude of our Δ_c of -200 ± 5 meV is well within the experimental results ranging from 160 to 217 meV (Refs. 31,32) whereas our Δ_s of 356 is only slightly larger compared to the range of 263–330 meV in the same references. These small disagreements could result from strain in the crystal used in the experiments. However, giving the error bar of the calculations these values are in very satisfactory agreement.

B. Optical transitions

The most widely used model for optical transition near the band gap considers transitions from the three upper VB to the lower three CB at Γ. It divides the transitions into three series of, in principle, identically spaced transitions labeled $\{A,B,C\}$, $\{A',B',C'\}$, and $\{A'',B'',C''\}$. Each series corresponds to transitions from the three VB to one CB with the lowest energy labeled as *A* and the highest energy as *C*. The unprimed series corresponds to the transition to the CBM $[\Gamma_6(1)]$; the primed series to the next CB $[\Gamma_7(3)]$; and the double-primed series to the third CB $[\Gamma_6(2)]$.

We here consider additional indirect (phonon-assisted) transitions series from the Γ point to other local minima in the BZ in particular the *N* and *T* points. We will call these series $\{A^N,B^N,C^N\}$, $\{A^T,B^T,C^T\}$, and $\{A^{T'},B^{T'},C^{T'}\}$. We will also consider direct transitions between the highest valence band and lowest conduction bands at the *N* and *T* points and will label these as D^N and D^T.

In Table II, we label the relevant energy levels discussed here using V (for VB) and C (for CB) with a subscript number counting from the band edge (V_1 means VBM; V_2 means first lower VB; C_1 means CBM; C_2 means first higher CB; etc.), and a superscript labeling the **k** point. The symmetry

TABLE II. Selected conduction and valence-band eigenvalues measured from valence-band maximum in $CdGeAs_2$.

State	Symmetry	LDA++ energy (eV)
C_3^Γ	$\Gamma_6(2)$	2.25
C_2^Γ	$\Gamma_7(3)$	1.79
C_1^Γ	$\Gamma_6(1)$	0.60
V_1^Γ	$\Gamma_7(4)$	0.00
V_2^Γ	$\Gamma_6(5)$	−0.15
V_3^Γ	$\Gamma_7(5)$	−0.46
C_1^T		1.80
C_2^T		2.10
C_1^N		1.05
V_1^T		−1.34
V_1^N		−0.73

label of each energy level is given in the second column. Using our calculated energy levels shown in Table II, we then examine various optical transition energies in Table III. In this table we also include information on the polarization dependence.

When spin-orbit coupling is neglected, the selection rules are determined by the single group. The allowed transitions are then

$$E\|c: \quad \Gamma_4\rightarrow\Gamma_1,\Gamma_5\rightarrow\Gamma_5,$$
$$E\perp c: \quad \Gamma_4\rightarrow\Gamma_5,\Gamma_5\rightarrow\{\Gamma_1,\Gamma_2,\Gamma_3,\Gamma_4\}. \tag{4}$$

On the other hand, when spin-orbit interaction is included the selection rules (of the double group) become

$$E\|c: \quad \Gamma_7\rightarrow\Gamma_6,\Gamma_6\rightarrow\Gamma_7,$$
$$E\perp c: \quad \Gamma_7\rightarrow\{\Gamma_6,\Gamma_7\}. \tag{5}$$

Strictly speaking, of course, we should only consider the selection rules of the double group. However, if spin-orbit coupling is not too strong, one may expect that transitions allowed in the double group but forbidden in the single group, will be weak. For example the $\Gamma_7(4)\rightarrow\Gamma_6(1)$ transition, which is the minimum band gap or A transition, is strictly speaking allowed for $E\perp c$ in the double group but is forbidden in the single group and is thus expected to be weak. On the other hand for $E\|c$, this same transition is allowed in both the single and double groups and is thus expected to be strong. In Table III we will indicate this as A for $E\|c$ meaning allowed in both single and double group or AF, allowed in double group but forbidden in single group, for $E\perp c$.

In Figs. 5 and 6 we compare our calculated spectrum with the experimental data. We caution that the height of the calculated peaks do not correspond to intensities, not even in a

TABLE III. Theoretical prediction of optical transitions peaks in the 0.5–3.0 eV range in $CdGeAs_2$.

Symbol	Energy (eV)	between	Polarization [a]	
			$E\|c$	$E\perp c$
A	0.60	$\Gamma_7(4)\rightarrow\Gamma_6(1)$	A	AF
B	0.75	$\Gamma_6(5)\rightarrow\Gamma_6(1)$	F	A
C	1.06	$\Gamma_7(5)\rightarrow\Gamma_6(1)$	AF	A
A'	1.79	$\Gamma_7(4)\rightarrow\Gamma_7(3)$	F	AF
B'	1.94	$\Gamma_6(5)\rightarrow\Gamma_7(3)$	AF	A
C'	2.25	$\Gamma_7(5)\rightarrow\Gamma_7(3)$	F	A
A''	2.25	$\Gamma_7(4)\rightarrow\Gamma_6(2)$	AF	AF
B''	2.40	$\Gamma_6(5)\rightarrow\Gamma_6(2)$	F	A
C''	2.71	$\Gamma_7(5)\rightarrow\Gamma_6(2)$	AF	A
		Phonon assisted transitions		
A^N	1.05	$\Gamma_7(4)\rightarrow C_1^N$		
B^N	1.20	$\Gamma_6(5)\rightarrow C_1^N$		
C^N	1.51	$\Gamma_7(5)\rightarrow C_1^N$		
A^T	1.80	$\Gamma_7(4)\rightarrow C_1^T$		
B^T	1.95	$\Gamma_6(5)\rightarrow C_1^T$		
C^T	2.26	$\Gamma_7(5)\rightarrow C_1^T$		
$A^{T'}$	2.10	$\Gamma_7(4)\rightarrow C_2^T$		
$B^{T'}$	2.25	$\Gamma_6(5)\rightarrow C_2^T$		
$C^{T'}$	2.56	$\Gamma_7(5)\rightarrow C_2^T$		
		Direct transitions at other **k** points		
D_N	1.78	$V_1^N\rightarrow C_1^N$		
D_T	3.14	$V_1^T\rightarrow C_1^T$		

[a]A: allowed, F: forbidden, AF: allowed in double group, forbidden in single group and hence weak.

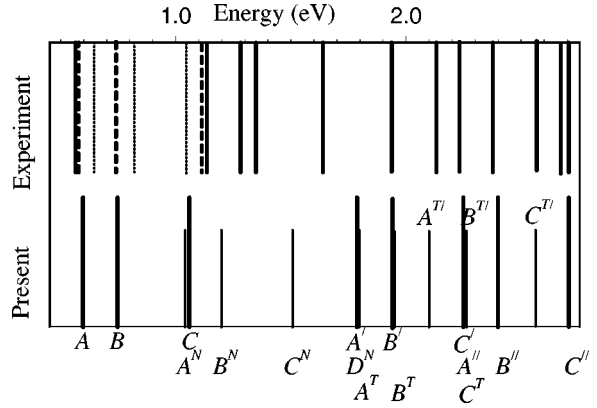

FIG. 5. Comparison of the optical transition levels predicted by our first principle band structure to the results from wavelength modulation (Ref. 9) (solid lines), electroreflectance (Ref. 8) (dashed lines), and photon e.m.f. (Ref. 7) (dotted lines). In our plot, two levels amplitude and line thickness distinguished the direct transitions from phonon-assisted transitions.

qualitative manner but only indicate the different nature of the transitions. In the first of these figures, we include the experimental data of Madelon *et al.*[9] as well as those of Krivaite *et al.*[8] and Borschevskii *et al.*[7] The reason why Madelon *et al.*[9] do not observe the *B* transition is not clear but is discussed in their paper.

While good agreement is obtained for the well established transitions *A*, *B*, and *C*,[7,8,13] the identification of the primed and double-primed series is more problematic. We note that the *A*, *B*, and *C* transitions basically provide us with information about the crystal field and spin-orbit splitting of the valence band, discussed in the previous section, but not with information about the conduction band splittings.

The *A* transition provides the minimum gap and the values for this range from 0.58 eV at room temperature,[8] to 0.65 eV at $T=77$ K.[13] An additional series with *A* at 0.57 eV was also found at $T=77$ K by Borschevskii *et al.*[7] but associated with a shallow acceptor to band transitions. The minimum gap at low temperature should thus be considered to be about 0.65 eV.

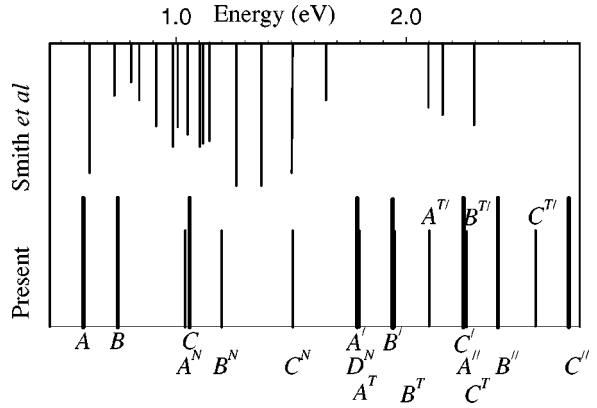

FIG. 6. Comparison of the optical transition levels predicted by our first principle band structure to the OAS results by Smith *et al.* (Ref. 31). The amplitudes of Smith *et al.*'s results reflected their actual measurement amplitude. In our plot, two levels amplitude and line thickness distinguished the direct transitions from phonon-assisted transitions.

We also note that the polarization dependence is in agreement with the measurements of Krivaite *et al.*[8] As predicted by our theory, the *A* peak is strong for $E\|c$ and weak for $E\perp c$. The *B* peak only is allowed for $E\perp c$ and the *C* peak is stronger for $E\perp c$ than for $E\|c$.

In Fig. 6 we compare our calculated spectrum with the recent data of Smith *et al.*[31] In this case, the peak heights of the experiment do correspond to measured intensities but the measurements are for unpolarized light. There are several more peaks in the low energy region than in the other experimental results. These are likely of extrinsic (defect related) origin. Also, the strong peaks in the region 1.2–1.6 eV were tentatively identified by these authors with Cr defect levels.

In contrast to the unprimed series, the primed and double-primed series have not been clearly identified experimentally. Either certain lines appear to be missing or additional lines not fitting in this simple description appear. Furthermore only a few studies consider the energy region above 1.2 eV.[9,31] A one-to-one correspondence between theoretical and experimental transitions appears impossible in the energy range above 1.2 eV. We believe the reasons for this are that (1) the primed and double-primed series correspond to weak pseudodirect transitions and (2) additional direct transitions appear in this same energy region.

Considering the other direct transitions, we note that the *N* state corresponds to the folded *L* state of ZB, which is usually associated with a strong saddlepoint transition (usually called the E_1 transition in ZB materials). In fact, we may note that the valence and conduction bands along the Γ-*N* direction near *N* are nearly parallel, indicating a high joint density of states. Thus, we can safely say that above this energy range direct transitions will clearly dominate indirect transitions. The direct transitions at *T* corresponding to folded direct transitions at *X* are at somewhat higher energy outside the range we wish to consider here.

On the other hand, the primed and double-primed series correspond to transitions to the folded *X* states of ZB. They are so-called pseudodirect and are hence expected to be rather weak. In fact, our previous study of $ZnGeP_2$ indicated that the momentum matrix elements for such transitions are very weak. The experimentally observed oscillator strengths for these transitions in $ZnGeP_2$ indicated the assistance of (zero momentum) phonons. They are thus similar to corresponding indirect transitions. In particular, we should note that the first two conduction bands at *T* correspond to the same ZB *X* states (X_{1c} and X_{3c}) as the folded Γ_{3c} and Γ_{2c}, respectively, except that these are the states corresponding to the *x* or *y* direction whereas the folded ones at Γ correspond to the *z* direction. They will thus have slightly different energy because of the chalcopyrite symmetry breaking between *z* and $\{x,y\}$, but one expects similar intensity between the indirect and pseudodirect transitions. In fact, we find that the indirect transitions from Γ to the lowest state at *T* coincides very nearly with the primed series, whereas the transitions to the second state at *T* lie somewhat below the double primed series.

TABLE IV. Conduction band effective masses in $CdGeAs_2$, in units of the electron mass.

Band	$m_\parallel$	$m_\perp$
$\Gamma_6(1)$	0.067	0.080
$\Gamma_6(2)$	1.780	0.319
$\Gamma_7(3)$	1.202	0.360

The A^N line of the indirect transitions from Γ to N coincides with the C transition. Possibly the Γ-N transitions may correpond to the transitions observed by Madelon *et al.* at 1.28, 1.35, and 1.64 eV if we allow for the possibility of a slight shift of the conduction band at N to slightly higher energy. Definitely, the uncertainty in our estimates of the gap corrections by at least 0.1 eV would allow this. However, it is not clear whether this weak indirect transition should be expected to be visible if other pseudodirect and indirect transitions are not observable.

Above 2 eV we definitely think it is no longer possible to identify the peaks in the reflectivity spectrum or its derivative as measured by Madelon *et al.*[9] with individual transitions at specific **k** points because we deal with a continuum of transitions. Rather a direct comparison with calculated $\varepsilon_2(\omega)$ or better reflectivity curves should be used. While $\varepsilon_2(\omega)$ curves were already reported in Ref. 3, a detailed analysis and comparison with the data remains to be done. We postpone this task for later work.

C. Conduction-band effective masses

The conduction band masses are obtained by directly fitting the first principles bands with parabola. The masses of the three CB studied are shown in Table IV. The lower CB has very little anisotropy and has a very light mass of $m_\parallel = 0.067\ m_e$ and $m_\perp = 0.080\ m_e$ as expected because of the small band gap. Our value is a factor two larger than the masses obtained by the empirical pseudopotential calculation ($0.03\ m_e$).[16] The only experimental estimate of the conduction band effective mass is based on differential thermoelectric power measurements and is $0.027\ m_e$.[11,12] Kildal[33] provided 4×4 $\mathbf{k}\cdot\mathbf{p}$ expressions for the mass in chalcopyrite semiconductors and used an estimated P momentum matrix element based on the average value of III-V compounds, which also gives values of $m_\parallel = 0.030\ m_e$ and $m_\perp = 0.039\ m_e$. This is most likely an underestimate because it does not include interactions with higher conduction bands. On the other hand, we should note that in narrow band gap semiconductors it is rather difficult to obtain reliable band masses. In particular, for GaAs, the LDA mass of $0.025\ m_e$ is well known to be strongly underestimated compared to the experimental value of $0.067\ m_e$, whereas the GW mass of $0.08\ m_e$ is slightly overestimated.

D. Valence-band effective Hamiltonian

Because of the three-fold degeneracy at Γ in ZB semiconductors in the absence of spin-orbit coupling, the effective masses are best described in terms of an effective 6×6 Hamiltonian (including spin degeneracy) as described in Luttinger's theory.[34] Here we discuss the extension of this model to chalcopyrite semiconductors.

Following the theory of invariants[35] the Hamiltonian is constructed from combinations of the angular momentum operator $\mathbf{L}$ (with $L=1$ describing the three-fold degeneracy of the states at Γ), the spin of the valence band electron $\boldsymbol{\sigma}$ and $\mathbf{k}$. All terms up to linear and quadratic in $\mathbf{k}$, L^2 and the spin-orbit coupling are included. Higher order relativistic terms involving $\boldsymbol{\sigma}$ and $\mathbf{k}$ or k^2 are neglected. Group theory allows us to classify the operator components according to their irreducible representations and to find those product combinations that are invariant, i.e., transform as the a_1 fully symmetric representation. Using the character tables and coupling coefficient tables of Koster *et al.*[29] we thus arrive at the following Hamiltonian for the point group D_{2d}:

$$\begin{aligned} H_{D_{2d}} &= \Delta_c L_z^2 + \Delta_s^\parallel L_z\sigma_z + \Delta_s^\perp (L_x\sigma_x + L_y\sigma_y) + A_1 k_z^2 \\ &\quad + A_2(k_x^2+k_y^2) + A_3 L_z^2 k_z^2 \\ &\quad + A_4(L_x^2+L_y^2)(k_x^2+k_y^2) + A_5(L_x^2-L_y^2)(k_x^2-k_y^2) \\ &\quad + A_6[L_x,L_y]k_xk_y + A_7([L_x,L_z]k_xk_z \\ &\quad + [L_y,L_z]k_yk_z) + A_8(L_xk_x + L_yk_y), \end{aligned} \tag{6}$$

in which L_x, L_y, L_z are the angular momentum operator components (in Cartesian coordinates), and $\sigma_x, \sigma_y, \sigma_z$ are the Pauli spin matrices and $[L_x,L_y]=(L_xL_y+L_yL_x)/2$. The above Hamiltonian can be written as the T_d symmetry Hamiltonian corresponding to the usual zinc blende semiconductors plus extra terms. The usual T_d Luttinger Hamiltonian is

$$\begin{aligned} H_{T_d} &= \frac{\Delta_s}{3}(\mathbf{L}\cdot\boldsymbol{\sigma}) + Ak^2 + (B-A)(L_x^2k_x^2 + L_y^2k_y^2 + L_z^2k_z^2) \\ &\quad - 2C([L_x,L_y]k_xk_y + [L_z,L_x]k_zk_x + [L_x,L_z]k_xk_z). \end{aligned} \tag{7}$$

We can identify $A=A_2$, $B-A=A_4+A_5$, and $-2C=A_6$. In addition to the usual T_d terms, there are then additional terms

$$\begin{aligned} H_{D_{2d}} &= H_{T_d} + (A_1-A_2)k_z^2 \\ &\quad + (A_3-A_4-A_5)L_z^2k_z^2 + (A_4-A_5)(L_x^2k_x^2 + L_y^2k_y^2) \\ &\quad + (A_7-A_6)([L_z,L_x]k_zk_x \\ &\quad + [L_y,L_z]k_yk_z) + A_8(L_xk_x + L_yk_y) + \Delta_c L_z^2 \\ &\quad + \left(\Delta_s^\parallel - \frac{\Delta_s}{3}\right)L_z\sigma_z + \left(\Delta_s^\perp - \frac{\Delta_s}{3}\right)(L_x\sigma_x + L_y\sigma_y). \end{aligned} \tag{8}$$

We introduce the notations $A'=A_1-A_2$, $A''=A_4-A_5$, $B'=A_3-A_4-A_5=A_3-B+A$, $A_7=-2C'$, $D=A_8$ for the extra terms. A quasicubic approximation consists in maintaining only the cubic A,B,C terms, the crystal field splitting and assuming that $\Delta_s^\parallel=\Delta_s^\perp=\Delta_s/3$. This approximation turns out to be fairly good. However the extra linear-in-**k** terms

TABLE V. Valence band effective mass expressions in terms of effective Hamiltonian parameters neglecting spin-orbit coupling and their values in $CdGeAs_2$. m_{4z} means the band connecting to the Γ_4 state in the z-direction. The relation with the expression in the fourth column is $m_{4z}=-(A+A')^{-1}$. The subscripts h and l stand for heavy and light.

k direction		m	$-m^{-1}=$	value of m (m_e)
$k_x=k_y=0,\ k_z\neq 0$	Γ-T	m_{4z}	$A+A'$	0.068
		m_{5z}	$B+A'+B'$	0.351
$k_y=k_z=0,\ k_x\neq 0$	Γ-H	m_{4x}	$B+A''-D^2/\Delta_c$	0.370
		m_{5xh}	$B+D^2/\Delta_c$	0.379
		m_{5xl}	$A+A''$	0.077
$k_z=0,\ k_x=k_y\neq 0$	Γ-N	m_{4xy}	$(2B+A''-2D^2/\Delta_c)/2$	0.349
		m_{5xyh}	$(A+A''+B-C+2D^2/\Delta_c)/2$	2.030
		m_{5xyl}	$(A+A''+B+C)/2$	0.068
$k_y=0,\ k_x=k_z\neq 0$	Γ-M	m_{4xz}	$(A+A'+A''+B-D^2/\Delta_c)/2$	0.148
		m_{5xzh}	$(2B+A'+B'+D^2/\Delta_c)/2$	0.368
		m_{5xzl}	$(A+B+A'+A''+B')/2$	0.103

with parameter A_8 have the effect of fully lifting the degeneracy of the bands in the $k_\perp$ plane into six distinct eigenvalues, i.e., they lead to a spin splitting. This also leads to the effect that the valence band maximum is slightly displaced from the Γ point.

Using as basis $|X\uparrow\rangle,|Y\uparrow\rangle,|Z\uparrow\rangle,|X\downarrow\rangle,|Y\downarrow\rangle,|Z\downarrow\rangle$, the form of the 6×6 matrix is

$$H=\begin{pmatrix} H_1 & 0 \\ 0 & H_1 \end{pmatrix}+\begin{pmatrix} H_{s\parallel} & H_{s\perp} \\ H_{s\perp}^{\dagger} & H_{s\parallel}^{*} \end{pmatrix}, \tag{9}$$

with the part without spin-orbit coupling

$$H_1=\begin{pmatrix} \Delta_c+(A+A'')k_x^2+Bk_y^2 & C'k_xk_y & Ck_xk_z+iDk_y \\ +(B+B'+A')k_z^2 & & \\ C'k_xk_y & \Delta_c+(A+A'')k_y^2+Bk_x^2 & Ck_yk_z-iDk_x \\ & +(B+B'+A')k_z^2 & \\ Ck_xk_z-iDk_y & Ck_yk_z+iDk_x & (A+A')k_z^2+(B+A'')(k_x^2+k_y^2) \end{pmatrix} \tag{10}$$

and the spin-orbit coupling parts

$$H_{s\parallel}=\begin{pmatrix} 0 & -i\Delta_s^{\parallel} & 0 \\ i\Delta_s^{\parallel} & 0 & 0 \\ 0 & 0 & 0 \end{pmatrix} \tag{11}$$

and

$$H_{s\perp}=\begin{pmatrix} 0 & 0 & \Delta_s^{\perp} \\ 0 & 0 & -i\Delta_s^{\perp} \\ -\Delta_s^{\perp} & i\Delta_s^{\perp} & 0 \end{pmatrix}. \tag{12}$$

For several special directions, and in the absence of spin-orbit coupling the bands can easily be obtained analytically to terms of order k_i^2. The results are summarized in Table V. The first-principles results without spin-orbit coupling along these directions are shown in Fig. 7. In Fig. 7, circles represent results along Γ-T and Γ-N while asterisks represent results along Γ-H and Γ-M (this direction is defined as $k_y=0$ and $k_x=k_z\neq 0$). We note that in the quasicubic model several simple relations hold for the masses in these directions. We also note that the parameter C' only produces terms of order k^4 which we neglect. This is because the C' couples states separated by the crystal field splitting whereas the terms in C couple two degenerate states at Γ.

We attempted to determine the eleven masses defined in Table V by simply performing parabolic fits to the first-principles eigenvalues, up to $k=0.04\ 2\pi/a$. For $k\leqslant 0.04\ 2\pi/a$, the first-principles values can be fitted very well by parabola in the first three directions listed in the table. However, this is not true for Γ-M direction, where the bands already diverge from parabolic behavior even at this small k value (see Fig. 7). This means that the expressions in Table V for the Γ-M direction hold only for an even smaller region near Γ. We thus decided not to use them in the fit.

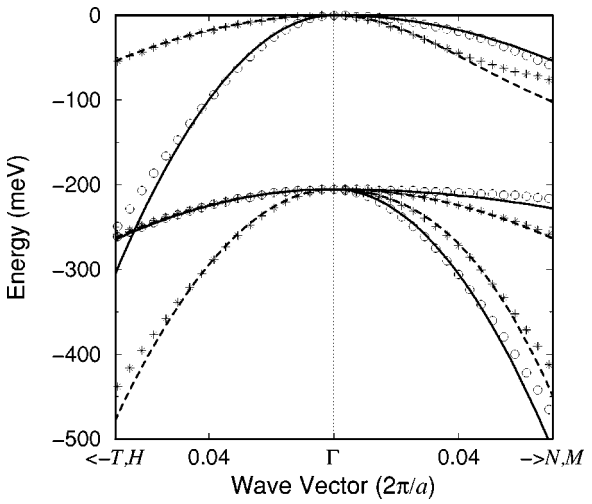

FIG. 7. Valence bands near maximum without spin-orbit coupling and their fit by the effective Hamiltonian for several directions. LMTO results: circles for Γ-T and Γ-N, asterisks for Γ-H and Γ-M. Full and dashed lines: best fit.

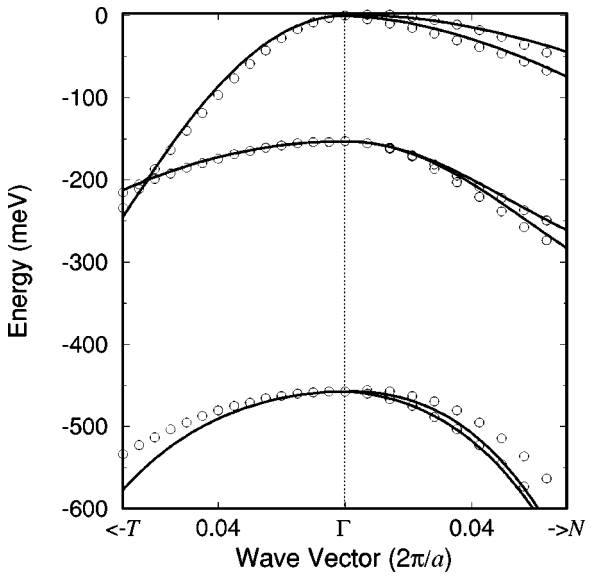

FIG. 8. Valence bands near maximum including spin-orbit coupling and their fit by the effective Hamiltonian. LMTO results: circles, effective Hamiltonian: full lines.

This left us with eight equations for seven unknowns. The next step is to determine the seven parameters A, B, C, A', A'', B', and D^2/Δ_c or D (since we already know Δ_c) by solving the list of equations shown in Table V.

We can see from Fig. 7 that the heavy mass band along the Γ-N direction is very flat, resulting in a larger error bar than the other bands. Therefore, we do not use this mass to determine the parameters. Now, we have seven equations with seven unknowns. However, the value of D^2/Δ_c is very small ($<0.01\ \hbar^2/2m_e$), compared to the accuracy of other parameters. Note that we can obtain D separately from the splitting of the bands when spin-orbit coupling is switched on, as shown below. Direct determination of the value of D^2/Δ_c from the equations in Table V, leads to a D^2/Δ_c with the wrong sign and diminished the accuracy of other parameters. We found it is better and perfectly accurate to set $D^2/\Delta_c=0$, while determining the other parameters. We use the first five equations in Table V to determine A, B, A', A'', and B' parameters. Then we solve the eighth equation in Table V for C. We obtain the values given in Table VI. With these parameters we can construct the complete effective Hamiltonian given in Eq. (9). To test the accuracy, we reproduce the band structures using this effective Hamiltonian. The results are shown as solid (for the Γ-T and Γ-N directions) and dashed (for the Γ-H and Γ-M directions) lines in Fig. 7. As we can see, the bands from the effective Hamiltonian match the first principles bands quite well inside the fitting area of $k \leqslant 0.04\ 2\pi/a$. Note especially the good agreement along the Γ-M direction which has not been used in the fitting. To further ensure that there is a good fit in all directions, we also compare the effective-Hamiltonian band structures to the first principles results on a regular mesh of points within a sphere of radius $k \leqslant 0.04\ 2\pi/a$ containing 290 points in total. The agreement is very impressive with the average error being less than 2 meV and the maximum error being less than 4 meV.

TABLE VI. Effective valence band Hamiltonian parameters.

Parameters and their values			units
A	B	C	
-12.974	-2.639	-13.778	$\hbar^2/2m_e$
A'	A''	B'	
-1.646	-0.064	1.436	$\hbar^2/2m_e$
D			
0.04			$e^2/2$
Δ_c	$\Delta_s^{\parallel}$	$\Delta_s^{\perp}$	
-205	114	119	meV

Next, we turn on the spin-orbit coupling in our first principles calculations and calculate the band structure using the same set of k points above. Adding the spin-orbit splitting obtained in Sec. III A to the effective Hamiltonian along with the above A, B, A', A'', and B' parameters we get an almost complete model for the band structures with spin-orbit coupling. The spin splitting in our model arises solely from the D parameter. We found that $D=0.04\ a_0\mathrm{Ry}$ gives the best fit between the model and the first principle results (note that $a_0\mathrm{Ry}=e^2/2$). We see that it provides a good match for the highest two bands but slightly less good for the crystal field split off band. This is probably due to the fact that we neglected higher relativistic terms coupling $\mathbf{k}$ with spin-orbit coupling. Nevertheless for the highest two valence bands, which are the most important for modeling transport, the agreement is quite good. On the set of 290 k points, we obtain an average error of less than 6 meV and the maximum error is less than 14 meV. The comparisons along two special directions are shown in Fig. 8. The effective masses at Γ along various directions are summarized in Table VII.

TABLE VII. Hole effective masses near band edges of $CdGeAs_2$ including spin-orbit coupling (in unit of m_e)

k direction	$m_{7(4)}$	$m_{6(5)}$	$m_{7(5)}$
Γ-T	0.078	0.351	0.219
Γ-N	0.290	0.128	0.141
Γ-H	0.290	0.128	0.141
Γ-M	0.122	0.187	0.172

IV. CONCLUSION

First-principles band structure calculations were carried out for $CdGeAs_2$ using the ASA-LMTO method including spin-orbit coupling and gap corrections. The results without spin-orbit coupling and strictly in the LDA were checked to be in agreement with those of FP-LMTO calculations. The underestimation of the band gap due to the LDA was corrected by shifting some of the ASA-LMTO Hamiltonian diagonal matrix elements using results for the parent compound GaAs as a guidance. We emphasize that the valence band splittings due to spin-orbit coupling and crystal field splitting are essentially not modified by this approach and are truly first-principles results. Good agreement with experiment is obtained for these splittings. The optical transitions in the vicinity of the fundamental gap were analyzed in a model going beyond the standard model which includes only transitions at Γ between the top three valence bands and the bottom three conduction bands. We point out, in particular, that the transitions to the higher two conduction bands, the so-called $A'B'C'$ and $A''B''C''$ series are weak pseudodirect transitions and should therefore be treated at the same level as corresponding indirect transitions from Γ to N and Γ to T. However, we caution that these series might be difficult to identify because from 1.8 eV on, other direct transitions start overwhelming the indirect transitions. Our values for the location of these higher energy transitions differ slightly from earlier work. A 6×6 effective Hamiltonian was derived to describe the valence band manifold using the theory of invariants and its parameters as well as the effective masses of the valence and conduction bands were obtained by fitting to the first-principles bands.

ACKNOWLEDGMENTS

Supported by the Air Force Office of Scientific Research under Grant No. F49320-00-1-0037. We thank S.R. Smith and M.C. Ohmer for making their paper available before publication.

*Currently at: Xerox Palo Alto Research Center, 3333 Coyote Hill Rd., Palo Alto, CA 94304.

[1] See, for example, M. C. Ohmer and R. Pandey, MRS Bull. **23**, 16 (1998) for an overview of the literature and history of this class of materials.

[2] J. L. Shay and J. H. Wernick, *Ternary Chalcopyrite Semiconductors: Growth, Electronic Properties, and Applications* (Pergamon Press, New York, 1975).

[3] S. N. Rashkeev, S. Limpijumnong, and W. R. L. Lambrecht, Phys. Rev. B **59**, 2737 (1999).

[4] L. E. Halliburton, G. J. Edwards, P. G. Schunemann, and T. M. Pollak, J. Appl. Phys. **77**, 435 (1995).

[5] R. Pandey, M. C. Ohmer, and J. D. Gale, J. Phys.: Condens. Matter **10**, 5525 (1998).

[6] J. B. Aufgang, D. Labrie, K. Olson, B. Paton, A. M. Simpson, G. W. Iseler, and A. Borshchevsky, Semicond. Sci. Technol. **12**, 1257 (1997).

[7] A. S. Borshchevskii, N. E. Dagina, A. A. Lebedev, K. Ovegov, I. K. Polushina, and Yu. V. Rud, Fiz. Tekh. Poluprov. **10**, 1905 (1976) [Sov. Phys. Semicond. **10**, 1136 (1976)].

[8] G. Krivaite, A. S. Borshchevskii, and A. Šileika, Phys. Status Solidi B **57**, K39 (1973).

[9] R. Madelon, M. Shaimi, A. Hairie, E. Paumier, and B. Mercey, Solid State Commun. **50**, 545 (1984).

[10] S. Isomura, S. Tarahashi, and K. Isomura, Jpn. J. Appl. Phys. **16**, 1723 (1977).

[11] N. A. Goryunova, A. S. Poplavnoi, Yu. I. Polygalov, and V. A. Chaldyshev, Phys. Status Solidi **39**, 9 (1970).

[12] N. A. Goryunova, F. P. Kesamanly, and É. O. Osmanov, Fiz. Tverd. Tela **5**, 2031 (1963) [Sov. Phys. Solid State **5**, 1484 (1963)].

[13] I. P. Akichemko, V. S. Ivanov, and A. S. Borshchevskii, Fiz. Tekh. Poluprov. **7**, 425 (1973) [Sov. Phys. Semicond. **7**, 309 (1973)].

[14] L. B. Zlatkin, E. V. Ivanov, G. F. Karavaev, and V. A. Chaldyshev, Fiz. Tekh. Poluprov **5**, 2058 (1971) [Sov. Phys. Semicond. **5**, 1794 (1972)].

[15] Yu. I. Polygalov and A. S. Poplavnoi, Izv. Vuzov, Fiz. **12**, 78 (1981).

[16] R. Madelon, E. Paumier, and A. Hairie, Phys. Status Solidi B **165**, 435 (1991).

[17] P. Zapol, R. Pandey, M. Seel, J. M. Recio, and M. C. Ohmer, J. Phys.: Condens. Matter **11**, 4517 (1999).

[18] S. Limpijumnong, W. R. L. Lambrecht, and B. Segall, Phys. Rev. B **60**, 8087 (1999).

[19] X. Zhu and S. G. Louie, Phys. Rev. B **43**, 14142 (1991).

[20] S. C. Abrahams and J. L. Berstein, J. Chem. Phys. **61**, 1140 (1974).

[21] P. Hohenberg and W. Kohn, Phys. Rev. **136**, B864 (1964); W. Kohn and L. J. Sham, *ibid.* **140**, A1133 (1965).

[22] L. Hedin and B. I. Lundqvist, J. Phys. C **4**, 2064 (1971).

[23] M. Methfessel, Phys. Rev. B **38**, 1537 (1988).

[24] H. J. Monkhorst and J. D. Pack, Phys. Rev. B **13**, 5188 (1976).

[25] O. K. Andersen, Phys. Rev. B **12**, 3060 (1975); O. K. Andersen, O. Jepsen, and M Šob, in *Electronic Band Structure and its Applications*, edited by Yussouf M (Springer, Heidelberg, 1987), p. 1.

[26] R. W. Godby, M. Schlüter, and L. J. Sham, Phys. Rev. B **37**, 10159 (1988).

[27] S. B. Zhang, D. Tománek, M. L. Cohen, S. G. Louie, and M. S. Hybertsen, Phys. Rev. B **40**, 3162 (1989).

[28] R. Sandrock and J. Treusch, Z. Naturforsch. A **19**, 844 (1964).

[29] G. F. Koster, J. O. Dimmock, R. G. Wheeler, and H. Statz, *Properties of the Thirty-two Point Groups* (M.I.T. Press, Cambridge, 1963).

[30] M. Lietz and U. Rössler, Z. Naturforsch. A **19**, 850 (1964).
[31] S. R. Smith, M. C. Ohmer, J. E. McCrae, P. G. Schunemann, and T. M. Pollak (unpublished).
[32] A. Shileika, Surf. Sci. **37**, 730 (1973).
[33] H. Kildal, Phys. Rev. B **10**, 5082 (1974).
[34] J. M. Luttinger, Phys. Rev. **102**, 1030 (1956); J. M. Luttinger and W. Kohn, *ibid.* **97**, 869 (1955).
[35] K. Cho, Phys. Rev. B **14**, 4463 (1976).